Dataset Documentation/Readme
Title: NASA HIWC 2022 GOES-16 Datasets and Animations

Author
Kristopher Bedka
Climate Science Branch, Science Directorate
NASA Langley Research Center
21 Langley Blvd, Mail Stop 420
Hampton, VA 23681
Phone: 757-375-9234
Email: kristopher.m.bedka@nasa.gov
ORCID: 0000-0003-3066-0555

1.0 Data Set Description

- Introduction or abstract
  This dataset detects and characterizes deep convective clouds, lightning activity, and potential locations of high ice water content using GOES-16 satellite imagery in support of the July 2022 NASA High Ice Water Content (HIWC 2022) campaign. GOES-16 Advanced Baseline Imager (ABI) and Geostationary Lightning Mapper (GLM) data are processed at 5-minute intervals and ~ 2 km pixel spacing over a geographic domain encompassing all of the DC-8 research flights using algorithms and statistical models developed at NASA Langley Research Center. The HIWC 2022 campaign was based in Jacksonville, Florida.

- Data version number and date
  Version 1

- Data Status (Preliminary or Final)
  Final

- Time period covered by the data
  HIWC 2022 Science Flights from 8 to 30 July 2022

- Physical location (including lat/lon/elev) of the measurement or platform
  geospatial_lat_min = " 16.01"
  geospatial_lat_max = " 39.99"
  geospatial_lon_min = "-92.99"
  geospatial_lon_max = "-66.01"

- Data Frequency - Frequency of data collection (e.g., 5 minute, hourly, continuous, etc.):
  5 Minute

- Data source (e.g., for operational data include agency), if applicable
  NOAA GOES-16 Advanced Baseline Imager and Geostationary Lightning Mapper

- Web address references (e.g., project web site, etc.), if applicable
  https://clouds.larc.nasa.gov/cgi-bin/site/showdoc?docid=4&cmd=field-experiment-homepage&exp=HIWC-2022

- Data set restrictions (i.e., indicate if data set needs to be restricted, requires password protection, contains personal info, description of any licensing, etc.)
  None

2.0 Instrument Description

- Brief text describing the instrument and how it collects data including references
  The Advanced Baseline Imager is the primary instrument on the GOES-R Series for imaging Earth's weather, oceans and environment. ABI views the Earth with 16 different spectral bands (compared to five on the previous generation of GOES), including two visible channels, four near-infrared channels, and ten infrared channels. For more information: https://www.goes-r.gov/spacesegment/abi.html

  The Geostationary Lightning Mapper is a single-channel, near-infrared optical transient detector that can detect the momentary changes in an optical scene, indicating the presence of lightning. GLM measures total lightning (in-cloud, cloud-to-cloud and cloud-to-ground) activity continuously over the Americas and adjacent ocean regions with near-uniform spatial resolution of approximately 10 km. For more information: https://www.goes-r.gov/spacesegment/glm.html

- Figures (or links), if applicable
  N/A

- Table of specifications (i.e., accuracy, precision, frequency, resolution, etc.)
  See web links immediately above

3.0 Data Collection and Processing

- Description of data collection
- Description of derived parameters and processing techniques used
  GOES-16 data is processed at 5 minute intervals using a set of NASA Langley Research Center algorithms and statistical models referenced in Section 6.0 below that are designed to detect and characterize deep convective clouds, lightning activity, and potential locations of high ice water content. GOES-16 data is gridded to a 56 pixel/degree resolution, which is near 2 km at latitudes where the DC-8 flew. Pixels with recent lightning activity, or those that comprise a highly textured region in the GOES-16 ABI 0.64 micron visible channel or a localized cold spot (based on GOES-16 ABI 10.3 micron channel) with temperatures near to or colder than the tropopause are considered to be convective updrafts capable of generating HIWC conditions at flight level. Cloud optical depth is derived during daylight hours using a statistical model applied to 0.64 micron data for regions considered to be convective anvil clouds.

Tropopause-relative IR temperature is derived by differencing the GOES-16 ABI 10.3 micron brightness temperature with a smoothed tropopause temperature analysis from the NASA MERRA-2 reanalysis. The distance to the nearest updraft region, the tropopause-relative IR temperature and cloud optical depth are combined using a statistical model to derive a HIWC probability. Cloud top height, pressure, and potential temperature are retrieved by matching anvil cloud temperature with a co-located MERRA-2 (interpolated in time to the GOES image time) temperature, height, and pressure profile. Parallax corrections in the latitudinal and longitudinal directions are derived based on a pixel's cloud top height to enable better matching with the aircraft location. GOES-16 lightning detections are aggregated over the 10-minute period ending at the time of the GOES ABI scan to quantify lightning activity.

Animations in MP4 format showing the DC-8 flight track overlaid on GOES visible, water vapor, and IR window imagery, and HIWC probability estimates are provided. Zoomed animations are also provided showing the DC-8 flight track and the mean IKP-2 total water content (at 45-second intervals) data over convective storms intensively sampled by the DC-8, showing relationships between GOES visible (upper-left below), Tropopause-IR temperature difference (upper right), visible texture detections (magenta contour, lower left) and detection of likely overshooting cloud top pixels (colors, lower-left), and HIWC probability (lower-right).

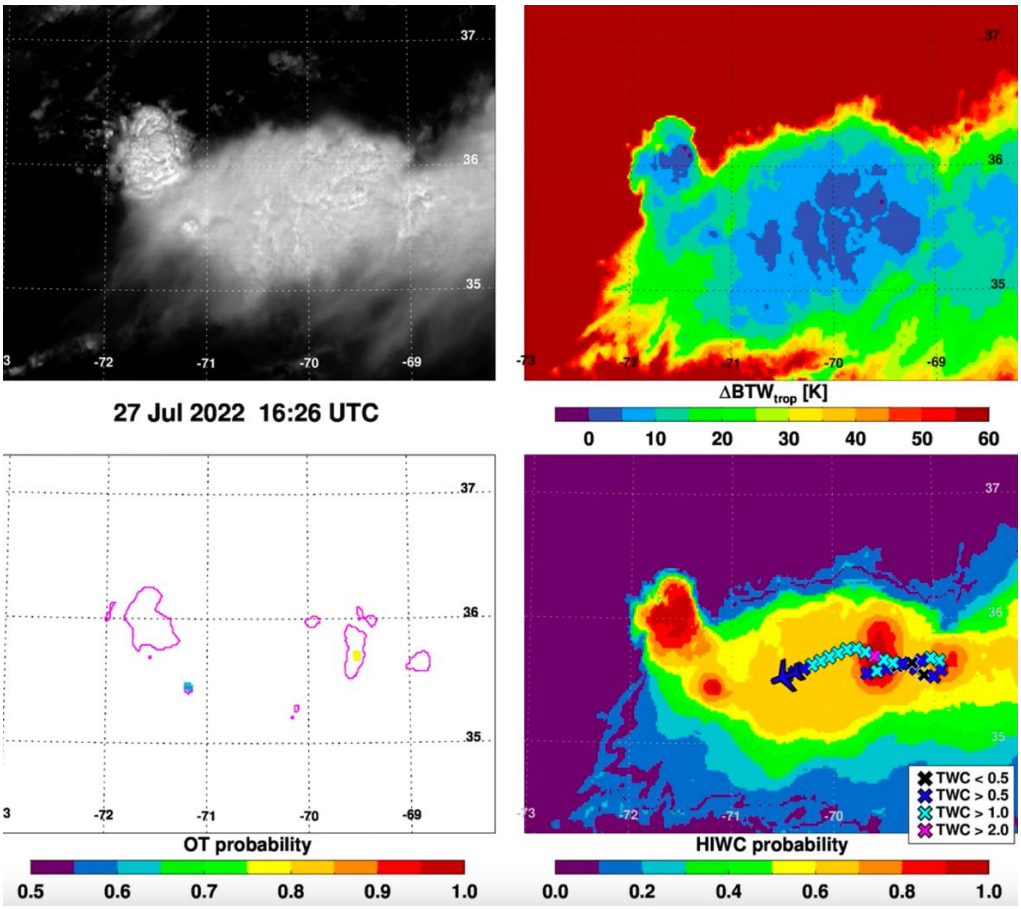

- Description of quality assurance and control procedures
  N/A

- Data intercomparisons, if applicable
  See comparisons below of various GOES satellite products, DC-8 aircraft altitude, and the mean IKP-2 total water content over 5 and 45-sec periods for a DC-8 flight on 27 July 2022

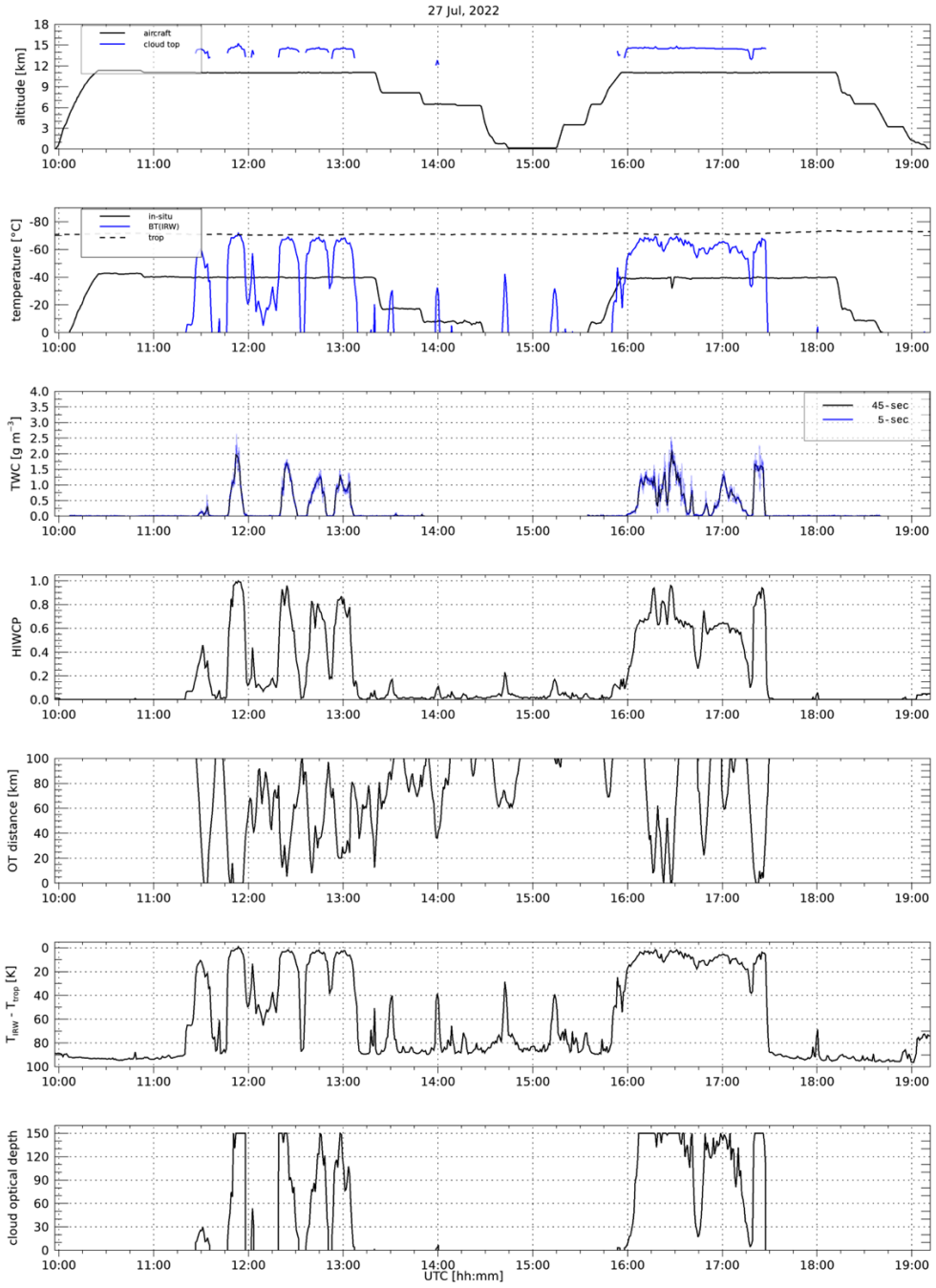

4.0 Data Format

- Data file structure and file naming conventions (e.g., column delimited ASCII, NetCDF, GIF, JPEG, etc.)
  NetCDF-4 and MP4
  NetCDF files are organized into tar archives for each DC-8 research flight day
  NetCDF files are named:
  NASALARC_GOES16_CONVECTION_DETECTION_YYYYDDD_HHMM.nc
  Where YYYY is year, DDD is day of year

  GOES_HIWC2022_HIWCProbability_TWC_animations.zip: Zoomed animations of DC-8 flight track, 45 sec IKP-2 TWC data, and GOES-derived products like the graphic shown in Section 3.0 above

  GOES_HIWC2022_flight_track_overlay_animations.zip: DC-8 flight track animations overlaid on GOES visible, water vapor, IR window, and HIWC probability data

- Data format and layout (i.e., description of header/data records, sample records)
- List of parameters with units, sampling intervals, frequency, range

```
dimensions:
        time = 1 ;
        nlines = 1344 ;
        npixels = 1512 ;
variables:
        double time(time) ;
                time:date_time_stamp = "2022-07-26T15:26:17Z" ;
                time:long_name = "Modified Julian Day of the Nominal Satellite Image Timestamp" ;
                time:units = "days since 1858-11-17T00:00:00.000" ;
                time:definition = "http://tycho.usno.navy.mil/mjd.html" ;
                time:comments = "MJD equals 51544.0 at Jan/01/2000 00:00" ;
        float latitude(nlines) ;
                latitude:long_name = "Latitude" ;
                latitude:scale_factor = 57.29578f ;
                latitude:_FillValue = -999.f ;
                latitude:units = "degrees_north" ;
        float longitude(npixels) ;
                longitude:long_name = "Longitude" ;
                longitude:scale_factor = 57.29578f ;
                longitude:_FillValue = -999.f ;
                longitude:units = "degrees_east" ;
        double scan_time(nlines) ;
                scan_time:long_name = "Observation Time (MJD) for Current Line" ;
                scan_time:units = "days since 1858-11-17T00:00:00.000" ;
                scan_time:definition = "http://tycho.usno.navy.mil/mjd.html" ;
                scan_time:comments = "MJD equals 51544.0 at Jan/01/2000 00:00" ;
        ushort ir_brightness_temperature(time, nlines, npixels) ;
                ir_brightness_temperature:long_name = "IR Brightness Temperature Image" ;
                ir_brightness_temperature:valid_range = 15000US, -30536US ;
                ir_brightness_temperature:units = "degrees_Kelvin" ;
                ir_brightness_temperature:scale_factor = 0.01f ;
                ir_brightness_temperature:_FillValue = -1US ;
                ir_brightness_temperature:coordinates = "longitude latitude time" ;
```

ubyte ot_probability(time, nlines, npixels) ;
ot_probability:long_name = "Overshooting Top Probability" ;
ot_probability:valid_range = 1UB, 100UB ;
ot_probability:units = "unitless" ;
ot_probability:_FillValue = 0UB ;
ot_probability:coordinates = "longitude latitude time" ;
ot_probability:scale_factor = 0.01f ;
ushort ot_id_number(time, nlines, npixels) ;
ot_id_number:long_name = "IR Overshooting Top Identification Number" ;
ot_id_number:valid_range = 1US, 9999US ;
ot_id_number:units = "unitless" ;
ot_id_number:_FillValue = 0US ;
ot_id_number:coordinates = "longitude latitude time" ;
ot_id_number:comments = "The IR Overshooting Top Identification Number field shows all pixels that belong to an individual overshooting top updraft region. The ID numbers apply uniquely to each satellite scan, i.e. ID number 1 in one scan will likely not be the same feature as ID number 1 in the next scan, and therefore cannot be used to track an overshooting top throughout its lifetime." ;
ubyte hiwc_probability(time, nlines, npixels) ;
hiwc_probability:long_name = "High Ice Water Content Probability" ;
hiwc_probability:valid_range = 1UB, 100UB ;
hiwc_probability:units = "unitless" ;
hiwc_probability:_FillValue = 0UB ;
hiwc_probability:coordinates = "longitude latitude time" ;
hiwc_probability:scale_factor = 0.01f ;
ushort distance_to_overshooting_top(time, nlines, npixels) ;
distance_to_overshooting_top:long_name = "Distance to Nearest Overshooting Cloud Top or any Pixel with Visible Detection Rating over 4" ;
distance_to_overshooting_top:valid_range = 0US, -2US ;
distance_to_overshooting_top:units = "kilometers" ;
distance_to_overshooting_top:_FillValue = -1US ;
distance_to_overshooting_top:coordinates = "longitude latitude time" ;
distance_to_overshooting_top:scale_factor = 0.01f ;
ushort cloud_optical_depth(time, nlines, npixels) ;
cloud_optical_depth:long_name = "Cloud Optical Depth" ;
cloud_optical_depth:valid_range = 0US, 15000US ;
cloud_optical_depth:units = "unitless" ;
cloud_optical_depth:_FillValue = -1US ;
cloud_optical_depth:coordinates = "longitude latitude time" ;
cloud_optical_depth:scale_factor = 0.01f ;
cloud_optical_depth:comments = "Cloud optical depth is derived based on the difference between the observed reflectance and a prediction of reflectance for anvil clouds given the pixel viewing, solar zenith, and relative azimuth angles. The anvil reflectance prediction is based on analysis of one year of anvil clouds observed by GOES-13, GOES-15, and Himawari-8. Spatial analyses and thresholding of IR brightness temperatures were combined to define anvil clouds as is described for the ir_anvil_detection variable above. Anvil pixels were filtered to ensure spatial homogeneity in reflectance and IR temperature. Reflectances are binned by angles and a kernel-based approach introduced by Roujean et al. (1992) is used to extrapolate anvil reflectance for bins with little to no samples. The observed minus predicted anvil reflectance is then statistically related to cloud optical depth derived using the Visible Infrared Solar-infrared Split-Window Technique (VISST) developed within the NASA LaRC CERES Cloud Subsystem (Minnis et al. 2011). An optical depth of 150 is the maximum value retrieved by VISST, which corresponds to a reflectance that is slightly brighter than predicted for anvils. The fit is exponential so optical depth rapidly drops for clouds darker than the anvil reflectance prediction. This approach is considered experimental at the present time and a publication describing it is currently in preparation." ;
ushort ot_anvilmean_brightness_temperature_difference(time, nlines, npixels) ;
ot_anvilmean_brightness_temperature_difference:long_name = "Overshooting Top Minus Anvil Brightness Temperature Difference" ;
ot_anvilmean_brightness_temperature_difference:valid_range = 1US, 5000US ;
ot_anvilmean_brightness_temperature_difference:units = "degrees_Kelvin" ;
ot_anvilmean_brightness_temperature_difference:_FillValue = 0US ;

ot_anvilmean_brightness_temperature_difference:coordinates = "longitude latitude time" ;
ot_anvilmean_brightness_temperature_difference:scale_factor = 0.01f ;
short parallax_correction_longitude(time, nlines, npixels) ;
parallax_correction_longitude:long_name = "Longitudinal Parallax Correction Based On Cloud Top Height Retrieval" ;
parallax_correction_longitude:valid_range = -32767s, 32767s ;
parallax_correction_longitude:units = "degrees_east" ;
parallax_correction_longitude:_FillValue = -32768s ;
parallax_correction_longitude:coordinates = "longitude latitude time" ;
parallax_correction_longitude:scale_factor = 0.001f ;
short parallax_correction_latitude(time, nlines, npixels) ;
parallax_correction_latitude:long_name = "Latitudinal Parallax Correction Based On Cloud Top Height Retrieval" ;
parallax_correction_latitude:valid_range = -32767s, 32767s ;
parallax_correction_latitude:units = "degrees_north" ;
parallax_correction_latitude:_FillValue = -32768s ;
parallax_correction_latitude:coordinates = "longitude latitude time" ;
parallax_correction_latitude:scale_factor = 0.001f ;
ushort tropopause_temperature(time, nlines, npixels) ;
tropopause_temperature:long_name = "Temperature of the Tropopause Retrieved from MERRA-2 Reanalysis" ;
tropopause_temperature:valid_range = 15000US, -30536US ;
tropopause_temperature:units = "degrees_Kelvin" ;
tropopause_temperature:_FillValue = -1US ;
tropopause_temperature:coordinates = "longitude latitude time" ;
tropopause_temperature:scale_factor = 0.01f ;
ushort cloud_top_height(time, nlines, npixels) ;
cloud_top_height:long_name = "Cloud Top Height Retrieved from MERRA-2 Reanalysis" ;
cloud_top_height:valid_range = 1US, -15536US ;
cloud_top_height:units = "kilometers" ;
cloud_top_height:_FillValue = -1US ;
cloud_top_height:coordinates = "longitude latitude time" ;
cloud_top_height:scale_factor = 0.001f ;
cloud_top_height:comments = "The retrieval of cloud top height is based on matching the infrared temperature of anvil cloud pixels with an interpolated numerical model profile. The tropopause defined by the numerical model using the WMO lapse-rate definition, and the temperature profile above the tropopause is modified to cool at a rate of 4.5 K/km for GOES-8 to -15, MTSAT-1R and -2, and Meteosat 8-11, 6 K/km for Himawari-8/9 and GOES-16/17, and 7.3 K/km for MODIS. The lapse rates are based on the findings of Griffin et al. (JAMC, 2016) and other empirical analyses. Modification of the temperature profile addresses situations where the IR temperature within overshooting tops or very cold anvils is colder than any temperature in the model profile, which would lead to non-retrieval of cloud height. The IR temperature to model matching process is only applied to pixels considered to be anvil clouds. It begins at the 500 hPa level and proceeds upward until the closest match between observation and model temperature is found. The hypsometric relation is employed in the vertical interpolation process. IR temperature and cloud top pressure is used to derive potential temperature. This approach is considered experimental at the present time, and validation using CALIPSO cloud height retrievals is ongoing." ;
ushort tropopause_height(time, nlines, npixels) ;
tropopause_height:long_name = "Height of the Tropopause Retrieved from MERRA-2 Reanalysis" ;
tropopause_height:valid_range = 1US, -15536US ;
tropopause_height:units = "kilometers" ;
tropopause_height:_FillValue = -1US ;
tropopause_height:coordinates = "longitude latitude time" ;
tropopause_height:scale_factor = 0.001f ;
tropopause_height:comments = "The retrieval of tropopause height and pressure is based on 4D interpolation of numerical model data. The hypsometric relation is employed in the vertical interpolation process." ;
ushort tropopause_pressure(time, nlines, npixels) ;
tropopause_pressure:long_name = "Pressure at the Tropopause Retrieved from MERRA-2 Reanalysis" ;

tropopause_pressure:valid_range = 1US, -15536US ;
tropopause_pressure:units = "hPa" ;
tropopause_pressure:_FillValue = -1US ;
tropopause_pressure:coordinates = "longitude latitude time" ;
tropopause_pressure:scale_factor = 0.01f ;
tropopause_pressure:comments = "The retrieval of tropopause height and pressure is based on 4D interpolation of numerical model data. The hypsometric relation is employed in the vertical interpolation process." ;
ushort cloud_top_pressure(time, nlines, npixels) ;
cloud_top_pressure:long_name = "Cloud Top Pressure Retrieved from MERRA-2 Reanalysis" ;
cloud_top_pressure:valid_range = 1US, -15536US ;
cloud_top_pressure:units = "hPa" ;
cloud_top_pressure:_FillValue = -1US ;
cloud_top_pressure:coordinates = "longitude latitude time" ;
cloud_top_pressure:scale_factor = 0.01f ;
cloud_top_pressure:comments = "The retrieval of cloud top pressure is based on matching the infrared temperature of anvil cloud pixels with an interpolated numerical model profile. The tropopause defined by the numerical model using the WMO lapse-rate definition, and the temperature profile above the tropopause is modified to cool at a rate of 4.5 K/km for GOES-8 to -15, MTSAT-1R and -2, and Meteosat 8-11, 6 K/km for Himawari-8/9 and GOES-16/17, and 7.3 K/km for MODIS. The lapse rates are based on the findings of Griffin et al. (JAMC, 2016) and other empirical analyses. Modification of the temperature profile addresses situations where the IR temperature within overshooting tops or very cold anvils is colder than any temperature in the model profile, which would lead to non-retrieval of cloud height. The IR temperature to model matching process is only applied to pixels considered to be anvil clouds. It begins at the 500 hPa level and proceeds upward until the closest match between observation and model temperature is found. The hypsometric relation is employed in the vertical interpolation process. IR temperature and cloud top pressure is used to derive potential temperature. This approach is considered experimental at the present time, and validation using CALIPSO cloud height retrievals is ongoing." ;
ushort cloud_top_potential_temperature(time, nlines, npixels) ;
cloud_top_potential_temperature:long_name = "Cloud Top Potential Temperature Retrieved from MERRA-2 Reanalysis" ;
cloud_top_potential_temperature:valid_range = 1US, -15536US ;
cloud_top_potential_temperature:units = "degrees_Kelvin" ;
cloud_top_potential_temperature:_FillValue = -1US ;
cloud_top_potential_temperature:coordinates = "longitude latitude time" ;
cloud_top_potential_temperature:scale_factor = 0.01f ;
cloud_top_potential_temperature:comments = "The retrieval of cloud top potential temperature is based on matching the infrared temperature of anvil cloud pixels with an interpolated numerical model profile. The tropopause defined by the numerical model using the WMO lapse-rate definition, and the temperature profile above the tropopause is modified to cool at a rate of 4.5 K/km for GOES-8 to -15, MTSAT-1R and -2, and Meteosat 8-11, 6 K/km for Himawari-8/9 and GOES-16/17, and 7.3 K/km for MODIS. The lapse rates are based on the findings of Griffin et al. (JAMC, 2016) and other empirical analyses. Modification of the temperature profile addresses situations where the IR temperature within overshooting tops or very cold anvils is colder than any temperature in the model profile, which would lead to non-retrieval of cloud height. The IR temperature to model matching process is only applied to pixels considered to be anvil clouds. It begins at the 500 hPa level and proceeds upward until the closest match between observation and model temperature is found. The hypsometric relation is employed in the vertical interpolation process. IR temperature and cloud top pressure is used to derive potential temperature. This approach is considered experimental at the present time, and validation using CALIPSO cloud height retrievals is ongoing." ;
ubyte ir_anvil_detection(time, nlines, npixels) ;
ir_anvil_detection:long_name = "Anvil Cloud Detection Using IR Brightness Temperature" ;
ir_anvil_detection:valid_range = 1s, 255s ;
ir_anvil_detection:units = "count" ;
ir_anvil_detection:_FillValue = 0UB ;
ir_anvil_detection:coordinates = "longitude latitude time" ;
ir_anvil_detection:comments = "This anvil rating indicates confidence in anvil detection, where values over 10 roughly correspond to human perception of anvil cloud extent and values over 100 indicate a very high level of confidence. The rating exploits the spatial uniformity of a BT-score, which is constructed from the difference between tropopause temperature and pixel\'s IR temperature. Spatial uniformity is estimated from the

characteristics of BT-score\'s regional histogram and subsequently adjusted by the presence of cold pixels nearby and other factors." ;
ubyte GLM_influence(time, nlines, npixels) ;
GLM_influence:long_name = "Time integrated spatial evolution of lightning influence based on GLM counts" ;
GLM_influence:valid_range = 1UB, 255UB ;
GLM_influence:units = "unitless" ;
GLM_influence:_FillValue = 255UB ;
GLM_influence:scale_factor = 1.f ;
GLM_influence:coordinates = "longitude latitude time" ;
GLM_influence:aggregation_minutes = 10US ;
GLM_influence:comments = "This emprical field estimates a spatio-temporal proximity of GLM flashes to a given pixel. Greater values mean that a greater number of lightning flashes happened in close proximity to the time of the GOES ABI image." ;
ushort GLM_flash_count(time, nlines, npixels) ;
GLM_flash_count:long_name = "Time aggregated GLM flash counts interpolated to the ABI grid" ;
GLM_flash_count:valid_range = 1US, -2US ;
GLM_flash_count:units = "count" ;
GLM_flash_count:_FillValue = -1US ;
GLM_flash_count:scale_factor = 1.f ;
GLM_flash_count:coordinates = "longitude latitude time" ;
GLM_flash_count:aggregation_minutes = 10US ;
ushort visible_reflectance(time, nlines, npixels) ;
visible_reflectance:long_name = "Visible Reflectance Image" ;
visible_reflectance:valid_range = 1US, -15536US ;
visible_reflectance:units = "percent" ;
visible_reflectance:_FillValue = -1US ;
visible_reflectance:coordinates = "longitude latitude time" ;
visible_reflectance:scale_factor = 0.01f ;
ubyte ot_rating_visible(time, nlines, npixels) ;
ot_rating_visible:long_name = "Visible Texture Detection Rating" ;
ot_rating_visible:valid_range = 1s, 255s ;
ot_rating_visible:units = "count" ;
ot_rating_visible:_FillValue = 0UB ;
ot_rating_visible:coordinates = "longitude latitude time" ;
ubyte visible_anvil_detection(time, nlines, npixels) ;
visible_anvil_detection:long_name = "Anvil Cloud Detection in Visible Band" ;
visible_anvil_detection:valid_range = 1s, 255s ;
visible_anvil_detection:units = "unitless" ;
visible_anvil_detection:_FillValue = 0UB ;
visible_anvil_detection:coordinates = "longitude latitude time" ;

// global attributes:
:title = "Geostationary Visible and Infrared Imager Deep Convective Storm Detection and Characterization Dataset From NASA Langley Research Center" ;
:summary = "This file contains products designed to identify 1) deep convective anvil clouds, 2) cold or textured updraft and gravity wave regions embedded within the anvils, and 3) areas where ice crystal icing due to high ice water content could occur using visible and infrared imager observations and numerical model analyses.\nAlgorithm development was sponsored by the NOAA GOES-R Risk Reduction Research Program, the NASA ROSES Severe Weather Research Program, the NASA Applied Sciences Disasters Program, the NASA Earth Venture DCOTSS mission, and the NASA ARMD Advanced Air Transport Technology Project." ;
:reference1 = "Khlopenkov, K. V., K. M. Bedka, J. W. Cooney, and K. Itterly, 2021: Recent Advances in Detection of Overshooting Cloud Tops from Longwave Infrared Satellite Imagery. Journal of Geophysical Research: Atmospheres, 126, e2020JD034359. https://doi.org/10.1029/2020JD034359" ;
:reference2 = "Cooney, J. W., Bedka, K. M., Bowman, K. P., Khlopenkov, K. V., and Itterly, K., 2021: Comparing Tropopause-Penetrating Convection Identifications Derived from NEXRAD and GOES over the Contiguous United States. Journal of Geophysical Research: Atmospheres, 126, e2020JD034319. https://doi.org/10.1029/2020JD034319" ;

:reference3 = "Yost, C. R., Bedka, K. M., Minnis, P., Nguyen, L., Strapp, J. W., Palikonda, R., Khlopenkov, K., Spangenberg, D., Smith Jr., W. L., Protat, A., and Delanoe, J., 2018: A Prototype Method for Diagnosing High Ice Water Content Probability using Satellite Imager Data, Atmos. Meas. Tech., 11, 1615-1637, https://doi.org/10.5194/amt-11-1615-2018" ;
:creator_name = "Kristopher Bedka and Konstantin Khlopenkov" ;
:creator_email = "kristopher.m.bedka@nasa.gov, konstantin.khlopenkov@nasa.gov" ;
:institution = "NASA Langley Research Center" ;
:date_created = "2022-10-17T20:40:46Z" ;
:platform = "GOES-16" ;
:sensor = "Advanced Baseline Imager" ;
:product_version = "3.0" ;
:license = "No constraints on data access or use" ;
:keywords = "EARTH SCIENCE > ATMOSPHERE > CONVECTIVE CLOUDS/SYSTEMS (OBSERVED/ANALYZED) > CUMULONIMBUS" ;
:keywords_vocabulary = "NASA Global Change Master Directory (GCMD) Earth Science Keywords, Version 8.6" ;
:spatial_resolution = "2.0 km" ;
:geospatial_lat_min = " 16.01" ;
:geospatial_lat_max = " 39.99" ;
:geospatial_lon_min = "-92.99" ;
:geospatial_lon_max = "-66.01" ;
:time_coverage_start = "2022-07-26T15:26:53Z" ;
:time_coverage_end = "2022-07-26T15:28:47Z" ;
:numerical_model_data_source = "MERRA-2" ;

- Description of flags, codes used in the data and definitions (i.e., good, questionable, missing, estimated, etc.)
  None

5.0 Data Remarks

- PI's assessment of the data (i.e., disclaimers, instrument problems, quality issues, etc.)
  None

- Missing data periods, if applicable
  N/A

- Software compatibility (i.e., list of existing software to view/manipulate the data plus software repository locations/links and responsible parties' contact information)
  Any software capable of reading NetCDF-4 or playing MP4 movies

6.0 References

- List of publications and documents (e.g., conference proceedings, publications, theses, reports, etc.) cited in this data set description and/or using this data set. Provide links, if available.
  Bedka, K., Yost, C., Nguyen, L., Strapp, J. et al., "Analysis and Automated Detection of Ice Crystal Icing Conditions Using Geostationary Satellite Datasets and In Situ Ice Water Content Measurements," *SAE Int. J. Adv. & Curr. Prac. in Mobility* 2(1):35-57, 2020, https://doi.org/10.4271/2019-01-1953

Cooney, J. W., Bedka, K. M., Bowman, K. P., Khlopenkov, K. V., and Itterly, K., 2021: Comparing Tropopause-Penetrating Convection Identifications Derived from NEXRAD and GOES over the Contiguous United States. Journal of Geophysical Research: Atmospheres, 126, e2020JD034319. https://doi.org/10.1029/2020JD034319

Khlopenkov, K. V., K. M. Bedka, J. W. Cooney, and K. Itterly, 2021: Recent Advances in Detection of Overshooting Cloud Tops from Longwave Infrared Satellite Imagery. Journal of Geophysical Research: Atmospheres, 126, e2020JD034359. https://doi.org/10.1029/2020JD034359

Yost, C. R., Bedka, K. M., Minnis, P., Nguyen, L., Strapp, J. W., Palikonda, R., Khlopenkov, K., Spangenberg, D., Smith Jr., W. L., Protat, A., and Delanoe, J., 2018: A Prototype Method for Diagnosing High Ice Water Content Probability using Satellite Imager Data, Atmos. Meas. Tech., 11, 1615-1637, https://doi.org/10.5194/amt-11-1615-2018